NATIONAL ADVISORY COMMITTEE FOR AERONAUTICS

TECHNICAL NOTE 3696

A STUDY OF THE HIGH-SPEED PERFORMANCE CHARACTERISTICS OF 90° BENDS IN CIRCULAR DUCTS

By James T. Higginbotham, Charles C. Wood, and E. Floyd Valentine

Langley Aeronautical Laboratory
Langley Field, Va.

Washington
June 1956

NATIONAL ADVISORY COMMITTEE FOR AERONAUTICS

TECHNICAL NOTE 3696

A STUDY OF THE HIGH-SPEED PERFORMANCE CHARACTERISTICS OF 90° BENDS IN CIRCULAR DUCTS

By James T. Higginbotham, Charles C. Wood, and E. Floyd Valentine

SUMMARY

The performance of four 90° bends in ducts of constant diameter with ratios of radius of curvature to diameter of 0.75, 1.00, 2.50, and 4.00 was investigated over a range of inlet Mach numbers extending up to the choking condition for both a thin and a thick inlet boundary layer. The variation of the measured longitudinal static-pressure gradients at low speed from those predicted by two-dimensional, incompressible, potential-flow theory was determined. It was found that an increase in the inlet boundary-layer thickness decreased the choking Mach number by a very small amount for each of the elbows and had little effect on the other performance parameters. It was concluded that, for the type of elbows tested, a mean radius-diameter ratio of approximately 2.50 would yield the greatest inlet choking Mach number with the least loss of static and total pressure.

INTRODUCTION

The thrust and general operation of jet propulsion systems are directly dependent on duct pressure losses and flow characteristics. Simple or compound elbows (or turns) frequently constitute part of the duct system in helicopters and conventional aircraft. Two of the general characteristics of such duct components are reductions in pressure recovery and establishment of nonuniform flows. A general research program has, therefore, been undertaken to study these duct elements, the objectives being to increase the inlet choking Mach number, improve the general performance, and attain satisfactory methods for designing efficient elbows.

Some of the parameters that are known to influence elbow performance are the radius-diameter ratio (ratio of radius of curvature to diameter of elbow), cross-sectional shape, longitudinal variation of cross-sectional area, wall contours, ducting at the inlet and exit, inlet boundary-layer conditions, Reynolds number, and Mach number. Weske

(ref. 1) conducted an extensive elbow investigation (summarized in ref. 2) at a low inlet Mach number which indicated that 90° elbows with elliptical cross sections have the lowest losses for an aspect ratio (ratio of height to width in the plane of symmetry) of about 2.5 and a mean radius-diameter ratio of about 2.5. These proportions were also optimum for rectangular bends operating at Reynolds numbers above about 500,000. Even elbows of optimum proportions, however, discharge nonuniform flow distributions, and many investigations (for instance, refs. 3 to 6) have been conducted at low speeds to determine the basic flow phenomena and means of improving the general performance. Young, Green, and Owen (ref. 7) tested 90° elbows of square and rectangular cross section up to choking inlet Mach numbers with a minimum of inlet boundary layer. The results showed that, of the elbows tested, the square elbow with a radius-diameter ratio of 2 produced the highest choking Mach number and the least increase in loss with increasing Mach number.

The purpose of the present investigation was to study the performance characteristics of conventional circular-arc 90° elbows of circular cross section with radius-diameter ratios from 0.75 to 4.00, up to choking inlet Mach numbers, for a very thick and a very thin inlet boundary layer. The following information was of particular interest: values of choking Mach number for the purpose of determining flow capacities of conventional circular bends, the effects of increasing inlet Mach number on performance parameters, and the variation of the measured longitudinal static-pressure gradients at low speed from those predicted by potential-flow considerations. The last item was determined in order to examine the possibility of using potential flow in designing elbow wall contours to produce a desired longitudinal pressure variation. The Mach number range covered by the tests was from about 0.20 to the choke condition, and the corresponding Reynolds number range based on the duct diameter was from 0.53×10^6 to 1.30×10^6.

SYMBOLS

A	aspect ratio, h/w
d	diameter of elbow, 3.122 in.
h	height of elbow perpendicular to plane of elbow turning radius
$\overline{M}$	mean Mach number $\left(\text{based on mass flow, duct area, and } \overline{p}_{t,0}\right)$
P_r	reference pressure ratio, $p_{t,v}/p_b$

p static pressure

$\bar{p}$ average of static pressures at four equally spaced points about a cross section through the elbow

p_t total pressure

$\bar{p}_t$ mean mass-weighted total pressure, $\dfrac{\int_0^{r_r} \rho u p_t r_r \, dr_r}{\int_0^{r_r} \rho u r_r \, dr_r}$

$\bar{q}_c$ mean impact pressure, $\bar{p}_t - \bar{p}$

R_0 Reynolds number at reference inlet station based on duct diameter

r radius of curvature of center line of elbow, in.

r_r radius of elbow

T_t total temperature of air, $^\circ F$ abs

u local stream velocity

u_{max} maximum local velocity at a given duct station

w width of elbow in plane of elbow turning radius

x longitudinal distance along elbow wall from reference inlet station, in.

y distance from duct wall, in.

$\dfrac{\overline{\Delta p}}{\bar{q}_{c,0}}$ static-pressure-drop coefficient, $\dfrac{\bar{p}_0 - \bar{p}}{\bar{q}_{c,0}}$

$\dfrac{\overline{\Delta p}_t}{\bar{q}_{c,0}}$ total-pressure-loss coefficient, $\dfrac{\bar{p}_{t,0} - \bar{p}_{t,1.5}}{\bar{q}_{c,0}}$ (see section entitled "Test Procedure and Data Presentation")

δ boundary-layer thickness

$\delta_{.95}$ boundary-layer thickness at $\frac{u}{u_{max}} = 0.95$

δ^* boundary-layer displacement thickness, $\int_0^{\delta} \left(1 - \frac{u}{u_{max}}\right) dy$

θ boundary-layer momentum thickness, $\int_0^{\delta} \frac{u}{u_{max}} \left(1 - \frac{u}{u_{max}}\right) dy$

$\frac{\delta^*}{\theta}$ boundary-layer shape parameter

ρ mass density

Subscripts:

b barometric pressure

c compressible

ch choking

max maximum

th theoretical

0 reference inlet station

i elbow inlet

e elbow exit

1.0 1.0 diameter downstream of elbow exit

1.5 1.5 diameters downstream of elbow exit

2.0 2.0 diameters downstream of elbow exit

v reference plane upstream of venturi

APPARATUS

A diagram of the test setup is shown in figure 1. Air flow from a blower passed through the 30-inch duct, several screens and conical reducers, a venturi, a boundary-layer duct, and the model elbow, and exhausted to the atmosphere at the exit of a conical diffuser. The boundary-layer-development pipe was a straight pipe of approximately 25 diameters' length with a smooth inside surface located between the venturi and the test elbow. It could be removed as desired to permit testing with a thin boundary layer to the elbow.

Four elbows of circular cross section, identical except for differences in the radius-diameter ratio, were tested. (See fig. 2.) The elbows were constructed of plastic and had circular-arc contours and smooth interior surfaces. Each elbow had a straight section of constant diameter on both the upstream and the downstream end. These sections were 1.84 and 2.67 diameters long, respectively. The junction between the test elbow and the venturi or between the elbow and the boundary-layer duct was smooth.

The elbow instrumentation is indicated in figure 3. Four traversing total-pressure tubes were located 90° apart at station 0, 1.44 diameters upstream of the inlet to the elbows. In the elbow with $r/d = 1.00$, four more tubes were located 1.5 diameters downstream of the elbow exit, and two were also located in the plane of the elbow turning radius at the elbow exit. Static-pressure orifices were located in each elbow along the top, bottom, inner, and outer walls.

TEST PROCEDURE AND DATA PRESENTATION

Parameters of interest in this investigation are choking Mach number, static-pressure drop, static-pressure distribution along the elbow walls, total-pressure loss, and exit velocity distribution. These parameters are referenced to variables at station 0.

Surveys of the flow at various Mach numbers were made at station 0 with the elbow replaced by a 2.75-inch straight section followed by a 6° diffuser. The mass flow and mean weighted total pressure computed from these surveys were calibrated against the mass flow obtained from the venturi and the static pressure (referred to as the reference total pressure) upstream of the venturi. The total-pressure tubes were then removed and the elbow and exit diffuser were set in place. Data were obtained at various Mach numbers up to and including the choking Mach number in order that the mass flow, pressure distribution, and so forth through the elbow could be determined.

One of the more important parameters is the choking Mach number $\bar{M}_{ch}$ which is defined as the maximum mean Mach number attainable at station 0 for a given configuration and condition. It is based on the mass flow measured through the venturi and the mass-weighted total pressure measured at station 0. The static-pressure drop $\overline{\Delta p}$ is the difference between the average static-pressure reading at station 0 and at a downstream station. The average static pressure is defined as the average of the readings obtained from four orifices equally spaced about the duct. For the $r/d = 1.00$ elbow, the total-pressure loss $\overline{\Delta p}_t$ is the difference between the mean mass-weighted values obtained from the total-pressure surveys at stations 0 and 1.5. Total-pressure surveys were not made for the other three elbows; consequently, $\overline{\Delta p}_t$ was obtained by a different procedure from that just described. For these three elbows, $\overline{\Delta p}_t$ was calculated from one-dimensional relationships, elbow cross-sectional area, and measured values of mass flow, total pressure $\bar{p}_{t,0}$, total temperature T_t, and the static pressure at station 1.5. The dynamic pressure $\bar{q}_{c,0}$ used to obtain the nondimensional coefficients $\overline{\Delta p}/\bar{q}_{c,0}$ and $\overline{\Delta p}_t/\bar{q}_{c,0}$ is based on the weighted mean total pressure $\bar{p}_{t,0}$, a rectangular velocity distribution, and the mass flow. The velocity distributions at stations e and 1.5 in the horizontal plane are available for the $r/d = 1.00$ elbow only and are presented in terms of $\sqrt{\frac{p_t - p}{\bar{q}_{c,0}}}$, a quantity which approximates the local velocity divided by the mean velocity at station 0. A straight-line static-pressure gradient was assumed from the inner to the outer duct wall at station e for the purpose of calculating the local impact pressure, while an average static pressure obtained from the four static-pressure orifices at station 1.5 was assumed for the downstream station. Both experimental and theoretical longitudinal static-pressure distributions along the wall are presented for each elbow. The theoretical distribution corresponds to potential incompressible flow and is obtained by a relaxation procedure described in references 8 and 9. The distributions are presented in terms of $\overline{\Delta p}/\bar{q}_{c,0}$ along the inner and outer wall for each elbow. The measured distribution is presented in the same terms for several low-speed runs for comparison purposes. For high inlet speeds the pressure distributions along each of the four walls (top, bottom, inner, and outer) are presented in terms of the ratio $p/p_{t,v}$ of the local static pressure to the upstream center-line reference total pressure for several values of $\bar{M}_0$.

RESULTS AND DISCUSSION

Inlet Conditions

The velocity profiles for two inlet Mach numbers (approximately 0.4 and 0.8) at each of two different boundary-layer conditions are presented in figure 4. The profiles, as measured along four radii, were symmetrical so that an average is presented. The boundary-layer parameters are tabulated in this figure for the thick boundary layer. The thin boundary layers were too small for accurate determination of the boundary-layer parameters with the instrumentation used. Decreases in the boundary-layer thickness were noted with increase in the Mach number for both boundary-layer cases. From the velocity profiles given in figure 4 it will be noted that the inlet conditions corresponded to roughly the thinnest and thickest layers obtainable practically.

Choking Mach Number

The Mach number $\overline{M}_O$ at station O for each of the elbows is presented in figure 5 as a function of the ratio P_r for the two boundary-layer conditions. For each elbow, the highest value of $\overline{M}_O$ reached when $\overline{M}_O$ is plotted against P_r is defined as the choking Mach number $\overline{M}_{ch}$. It is observed from these curves that the elbows which had the largest choking Mach number required less total pressure to attain it and less pressure to attain any Mach number below the choke value.

A cross plot of the choking Mach number $\overline{M}_{ch,O}$, as a function of the elbow radius-diameter ratio r/d is shown in figure 6 for both boundary-layer test conditions. Also included in this figure are the results of reference 7 for square and rectangular elbows with a thin inlet boundary layer. The data show that somewhat higher choking Mach numbers were achieved for the circular elbows than for the square or rectangular ones. Whether this result indicates a fundamental difference in the flow development or a lack of comparability of the two sets of test data is unknown. For circular elbows, an increase in the inlet boundary-layer thickness decreased the choking Mach number slightly. The elbow with $r/d = 2.50$ is shown to produce the highest value of $\overline{M}_{ch}$ for both boundary-layer conditions ($\overline{M}_{ch} = 0.77$ for the thin boundary layer and $\overline{M}_{ch} = 0.75$ for the thick one). The value of $\overline{M}_{ch} = 0.77$ corresponds to 95 percent of the air flow obtainable at a Mach number of 1.00. A brief investigation of the use of vortex generators and vanes for increasing $\overline{M}_c$ was unproductive. More information is needed on control devices in elbows at high subsonic Mach numbers. For mechanical reasons, investigations of this nature should be made on elbows of larger scale.

Static-Pressure Distributions and Static-Pressure-Drop Coefficients

The static-pressure variation along the inner, outer, top, and bottom walls is presented in figure 7 for each elbow at both boundary-layer conditions for a range of inlet Mach numbers $\bar{M}_0$ from 0.20 to choke. The curves of static-pressure distribution through each elbow remain similar as the inlet Mach number is increased up to the Mach number where local shock waves (as indicated by the static-pressure distribution) occur in or downstream of the bend. Sonic velocities and, probably, local shocks occur in the region next to the inner wall of each elbow at values of $\bar{M}_0$ substantially below choke for the $r/d = 0.75$ and 1.00 elbows. This is not the case for the bends with larger radii. Changes in the radius-diameter ratio of the bends produce large changes in the magnitude of the pressure variations through the bends. For each elbow, the pressure field of the bend extends a considerable distance both upstream of the elbow inlet and downstream of the exit; however, in all cases, the influence of the elbow does not extend as far as the reference station 0.

The curves permit some conclusions relative to the point in the duct where choke occurred. The curves for the $r/d = 0.75$ and 1.00 elbows (top, bottom, and outer walls) indicate that sonic velocity was not reached in the elbow with either boundary layer. The values of $p/p_{t,v}$ for the inner-wall curve for these two elbows do not correspond to a representative local Mach number because of the high total-pressure loss along this wall. It is evident from these curves that choking must occur at the elbow exit or downstream of it. The high-speed curves indicate that the region downstream of the exit contains a mixture of subsonic and supersonic flow. At the 0.50-diameter location downstream of the exit, supersonic flow is present along the four walls for the $r/d = 0.75$ and the $r/d = 1.00$ elbow for both inlet boundary-layer conditions. It would be expected that choking would occur prior to the establishment of the supersonic flow that is noted at the 0.50-diameter downstream location. Also, it would seem logical for the choke location to correspond to a section which contains slightly subsonic and slightly supersonic flow in order to pass a maximum flow in a mixed flow stream. The approximate location of such sections falls between the elbow exit and the 0.50-diameter downstream location for each case. The curves for the elbows of $r/d = 2.50$ and 4.00 indicate that no section produced a Mach number of 1.00; therefore, it is concluded that choke occurred at the tailpipe exit of these elbows. These observations lead to the conclusion that the choking Mach numbers measured for the $r/d = 0.75$ and 1.00 elbows are representative because the choking section was close to the exit. However, the choking Mach numbers observed for the $r/d = 2.50$ and $r/d = 4.00$ elbows were determined partially by the length of the downstream straight section, so that shorter lengths might have produced slightly higher choking Mach numbers.

The static-pressure drop from station 0 to the elbow exit and to stations 1.0 and 2.0 is presented as a function of the inlet Mach number in figure 8. The elbow with $r/d = 2.50$ produced the lowest $\overline{\Delta p}/\bar{q}_{c,0}$ values for both boundary-layer conditions at each of the station locations. This fact, when considered with the choking Mach number data, is a further indication that the $r/d = 2.50$ elbow had the most favorable performance of the elbows tested. The static-pressure drop for the $r/d = 0.75$ and 1.00 elbows is controlled primarily by separation of the flow from the inner wall, whereas friction is the primary cause of loss in the $r/d = 4.00$ elbow. The increase in static-pressure-drop coefficient with inlet Mach number is more rapid for the elbows of lower r/d, where separation is the controlling factor. The pressure-drop coefficient for the $r/d = 2.50$ elbow increases until it is approximately equal to that of the $r/d = 4.00$ elbow at the choking condition for most of the measuring stations. The coefficients for the $r/d = 2.50$ and 4.00 elbows increase between stations e and 2.0, probably because of wall friction and mixing losses. In the $r/d = 0.75$ and 1.00 elbows, the coefficient rises between stations e and 1.0 and then decreases between stations 1.0 and 2.0. This result probably indicates that considerable turbulence and mixing losses with separated flow occur between stations e and 1.0 and that static-pressure recovery is obtained by the increasing uniformity of the velocity distribution between stations 1.0 and 2.0.

Total-Pressure-Loss Coefficient

Both the measured and the calculated total-pressure loss from station 0 to station 1.5 are presented in figure 9 for the $r/d = 1.00$ elbow. Within the scatter of the data points, one curve represents the two boundary-layer conditions for both the measured and the calculated losses. For this elbow $\overline{\Delta p}_t/\bar{q}_{c,0}$ increased from 0.24 at $\bar{M}_0 = 0.275$ to 0.33 at the choke Mach number. The greatest differences between calculated and measured values occurred with the thicker boundary layer. This fact indicates a less uniform velocity profile at station 1.5 with the thick boundary layer than with the thin one. The static-pressure drop to this station is also plotted for both boundary-layer conditions and indicates clearly the larger static-pressure drop at the higher Mach numbers.

A comparison of the total-pressure-loss coefficients for each of the elbows is presented in figure 10. The faired curves represent a mean of the losses noted for the thick and the thin inlet-boundary-layer condition. A quantitative evaluation of the effects of inlet-boundary-layer thickness is impossible because of the data scatter, particularly for the $r/d = 2.50$ and 4.00 elbows; however, it may be stated that the effect is small. The same trends are noted for the total-pressure-loss coefficient as for the static-pressure-drop coefficient; that is, the loss increases with Mach number increase, the smallest loss being

realized for the $r/d = 2.50$ elbow. The $r/d = 0.75$ elbow produced the highest losses and the most severe Mach number effect. At the choke condition, the elbow with $r/d = 2.50$ produced a total-pressure-loss coefficient of 0.16 as compared with 0.69 for the elbow with $r/d = 0.75$. The loss through the $r/d = 0.75$ elbow, $0.69\bar{q}_{c,0}$ or $0.136\bar{p}_{t,0}$, is equivalent to that through a normal shock at $\bar{M}_0 = 1.68$.

The longitudinal static-pressure distributions indicate that choking occurred downstream of the elbows. This result suggests that choking is obtained because of the loss in total pressure and the consequent change in density, in a manner similar to that for a long straight pipe. In order to check this hypothesis, the choking Mach number for the $r/d = 1.00$ elbow was calculated by using the measured loss coefficient at choke (fig. 10), one-dimensional compressible-flow equations, and the assumption that sonic velocity occurred at station 1.5. The resulting theoretical choking Mach number is shown in figure 10 and agrees closely with the thin-boundary-layer data. Unfortunately, the measured loss coefficients for the other elbows are not available; thus an adequate check of the above hypothesis is not possible. Agreement of the theoretical Mach number with the measured value for the $r/d = 1.00$ elbow, however, suggests the possibility of estimating the choking Mach number for a particular elbow design from a low-speed value of loss coefficient and an assumption regarding the effect of inlet speed on loss coefficient. According to the data of figure 10 for the thin boundary layer, increasing the inlet Mach number from 0.3 to choke increases the loss coefficient for elbows with $r/d = 0.75$, 1.00, 2.50, and 4.00 by 114, 33, 31, and 7 percent, respectively.

Downstream Velocity Distributions

For the $r/d = 1.00$ elbow, total-pressure surveys were made in the horizontal plane at stations e and 1.5 and the resulting data are presented in the form of velocity distributions in figure 11. As pointed out previously, a linear static-pressure distribution from the inner to the outer wall was assumed at station e and an average of four static-pressure readings about the elbow was used for station 1.5 in order to compute the velocity ratios at these stations. At the elbow exit (station e), separation is noted over about 12 to 15 percent of the diameter. The remainder of the flow is at an approximately constant total pressure, the velocity gradient being produced by the static-pressure variation. The flow at this point for high inlet Mach numbers consists of a mixture of subsonic and supersonic flow with a Mach number range from 0 to approximately 1.25. At station 1.5 the flow is considerably more uniform and all subsonic. The effect of the thick inlet boundary layer is shown most clearly at this station, where the low velocity region is more extensive than for the thin boundary layer.

The general increase in the relative velocity with increasing inlet Mach number, as shown in the distribution, is the primary result of the increasing difference in density between stations 0 and e or 1.5 with increasing Mach number.

Theoretical and Experimental Longitudinal Pressure Distributions

The theoretical distributions along the inner and outer walls of each elbow were calculated according to the relaxation method (refs. 8 and 9) for two-dimensional, incompressible, potential flow, and are presented in figure 12. These theoretical curves indicate normal pressure changes for such elbow designs, that is, an acceleration followed by an expansion along the inner wall and an expansion followed by an acceleration along the outer wall. The curves also indicate that the pressure gradient extends beyond the elbow inlet and exit both upstream and downstream. The radius-diameter ratio of the bends determines the magnitude of the transverse gradient in the bend since, owing to the centrifugal-force relationship, pressure differences across the bend are roughly inversely proportional to the radius-diameter ratio.

A comparison of the theoretical and experimental distributions for the thin-boundary-layer case is shown in figure 13. Only the thin-boundary-layer case is shown because it most closely approximates potential flow. The figure indicates excellent agreement on the outer wall for the $r/d = 0.75$, 1.00, and 2.50 elbows, where the boundary layer is continuously removed by the secondary flow, up to a point near the exit where the effects of the losses through the elbow are noted. Agreement was less satisfactory on the inner wall where the boundary layer accumulated as a result of the secondary flow and separation; however, the differences between the theoretical and experimental values follow the same trends, the actual flow producing roughly 75 percent more maximum pressure variation for the bends of small radius-diameter ratio. It should be noted that some of the differences between the theoretical and measured values may be accounted for by the fact that the theoretical distribution was computed by using the assumption of two-dimensional flow, which would not apply accurately to a circular elbow.

CONCLUSIONS

Four 90° constant-diameter circular-arc elbows with a straight pipe 2.67 diameters long attached to the exit were tested up to choking Mach numbers for a very thin and a very thick inlet boundary layer. The

ratio of the radius of curvature to the diameter (r/d) of the elbows was from 0.75 to 4.00 and the Reynolds number range was from 0.53×10^6 to 1.30×10^6. The following conclusions are derived:

1. The elbow with $r/d = 2.50$ produced the best performance with respect to total-pressure-loss coefficient, static-pressure drop, and choking Mach number. For the thin-boundary-layer case, the elbow attained a choking Mach number of 0.77 which corresponds to 95 percent of the maximum theoretical air flow obtainable.

2. Thickening the inlet boundary layer produced somewhat less uniform flow distributions downstream of the elbows but did not affect appreciably the pressure losses and choking Mach number.

3. Longitudinal wall static-pressure gradients indicate that the elbows with $r/d = 0.75$ and 1.00 choked in the tailpipe in a section extending from the elbow exit to 0.5 diameter downstream. The two elbows with large radius-diameter ratios choked at the end of the 2.67-diameter length of tailpipe.

4. At the choke condition, the elbow with $r/d = 2.50$ produced a total-pressure-loss coefficient of 0.16 as compared with 0.69 for the elbow with $r/d = 0.75$. As the inlet Mach number was increased from 0.3 to the choking value, the loss coefficient for the elbow with $r/d = 2.50$ increased 31 percent; whereas, the loss coefficient for the elbow with $r/d = 0.75$ increased more than 100 percent.

5. Longitudinal pressure distributions computed by using incompressible, two-dimensional, potential-flow theory were in excellent agreement with the measured pressure distributions along the outer wall for the $r/d = 0.75$, 1.00, and 2.50 elbows. Agreement along the inner wall was poor because of secondary flow and flow separation in the elbows.

Langley Aeronautical Laboratory,
National Advisory Committee for Aeronautics,
Langley Field, Va., February 28, 1956.

REFERENCES

1. Weske, John R.: Pressure Loss in Ducts With Compound Elbows. NACA WR W-39, 1943. (Formerly NACA ARR, Feb. 1943.)

2. Henry, John R.: Design of Power-Plant Installations. Pressure-Loss Characteristics of Duct Components. NACA WR L-208, 1944. (Formerly NACA ARR L4F26.)

3. Valentine, E. Floyd, and Copp, Martin R.: Investigation To Determine Effects of Rectangular Vortex Generators on the Static-Pressure Drop Through a 90° Circular Elbow. NACA RM L53G08, 1953.

4. Patterson, G. N.: Note on the Design of Corners in Duct Systems. R. & M. No. 1773, British A.R.C., 1937.

5. Weske, John R.: Experimental Investigation of Velocity Distributions Downstream of Single Duct Bends. NACA TN 1471, 1948.

6. Palme, Hans Olaf: An Investigation of the Effect of Boundary Layer Suction on the Air Resistance in Channel Elbows. KTH-Aero TN 2, Roy. Inst. of Tech., Div. of Aero., Stockholm, Sweden, 1948.

7. Young, A. D., Green, G. L., and Owen, P. R.: Tests of High-Speed Flow in Right-Angled Pipe Bends of Rectangular Cross-Section. R. & M. No. 2066, British A.R.C., 1943.

8. Southwell, R. V.: Relaxation Methods in Engineering Science. A Treatise on Approximate Computations. The Clarendon Press (Oxford), 1940.

9. Emmons, Howard W.: The Numerical Solution of Compressible Fluid Flow Problems. NACA TN 932, 1944.

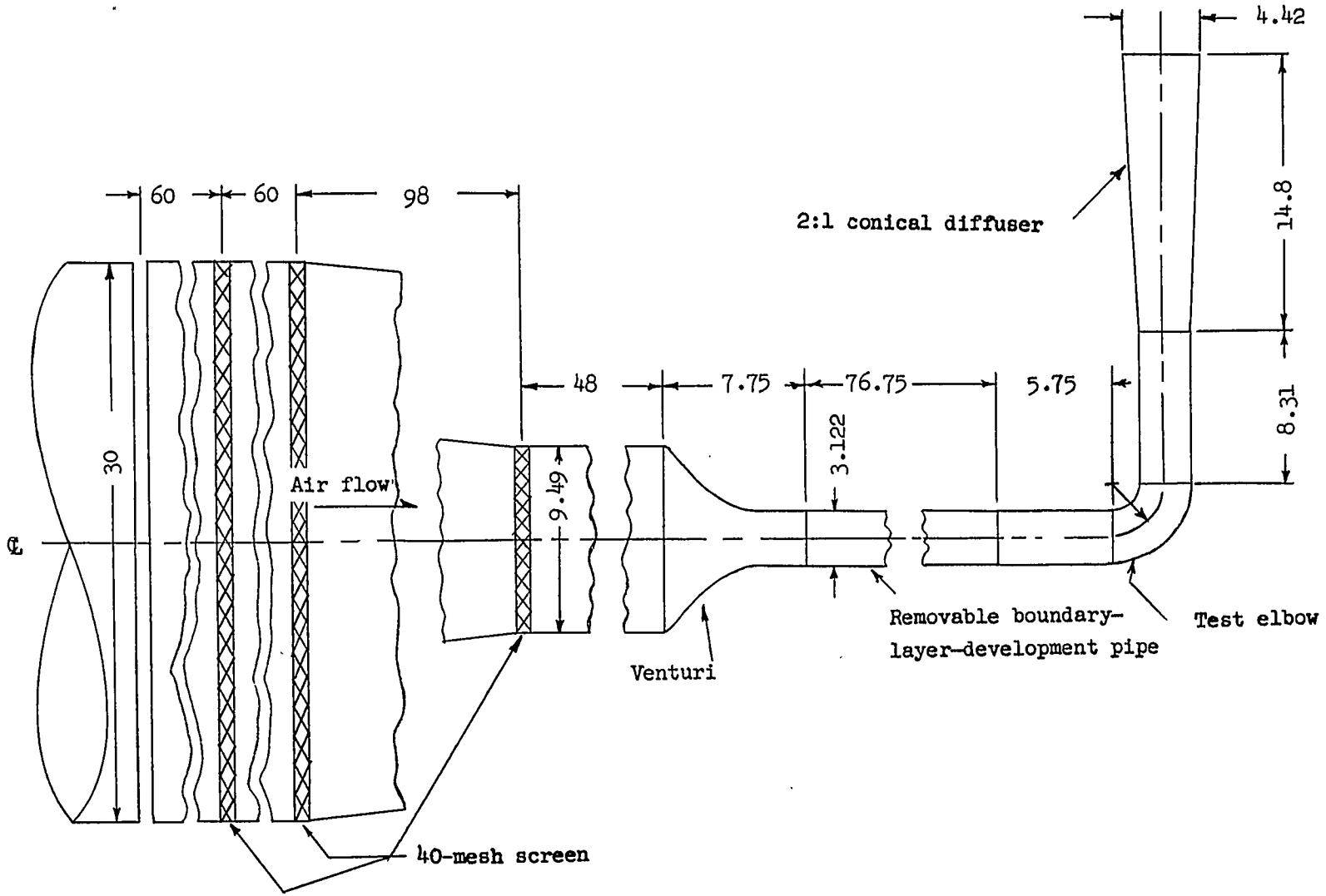

Figure 1.- Diagram of test arrangement. All dimensions are in inches.

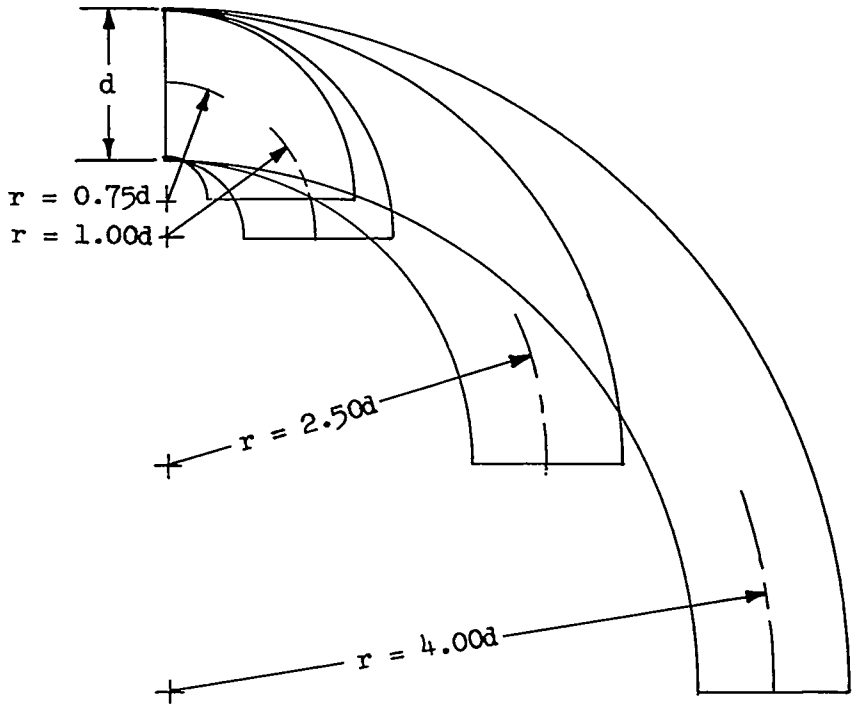

Figure 2.- Diagram of the four elbows tested.

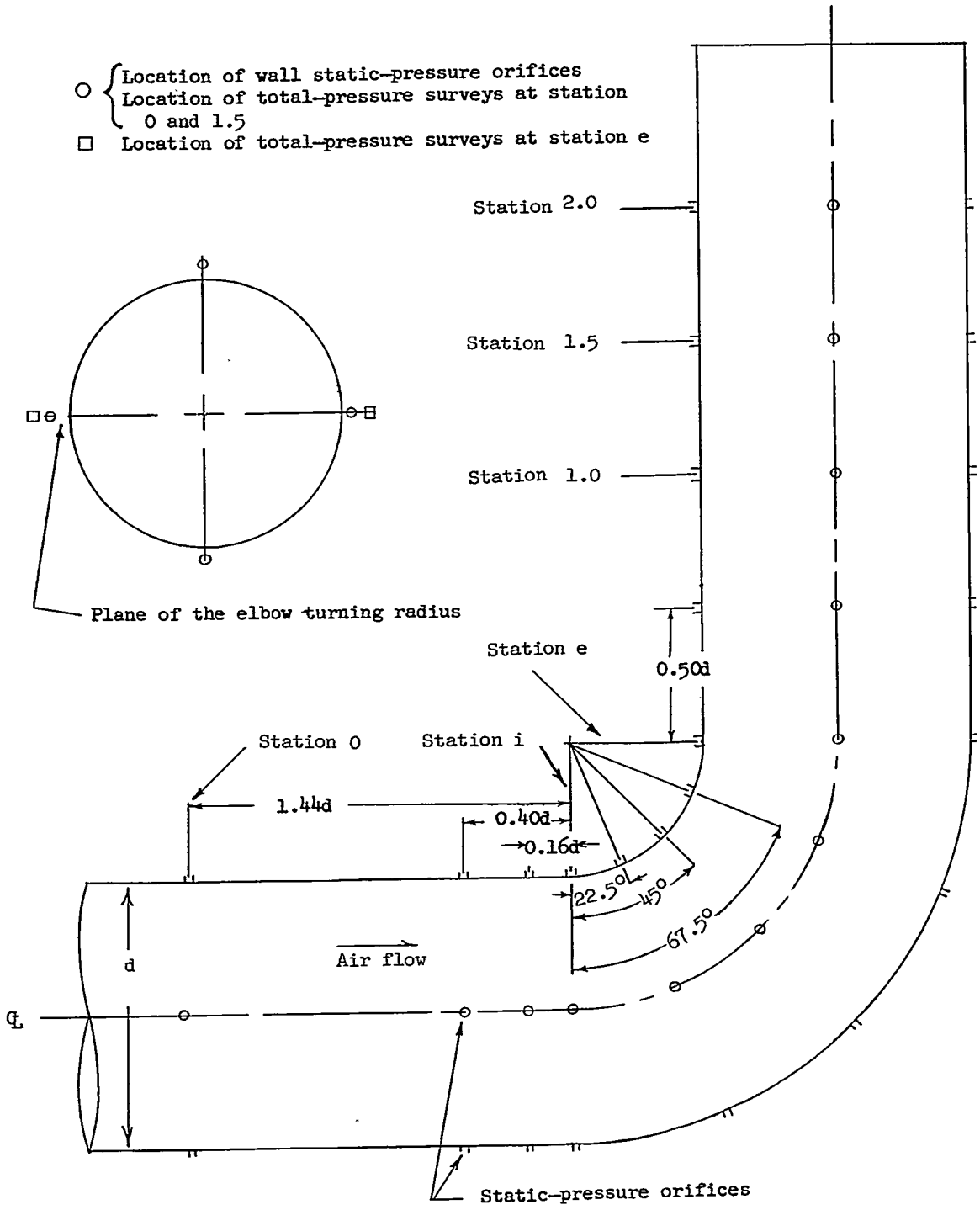

Figure 3.- Diagram of test elbow showing locations of instrumentation.

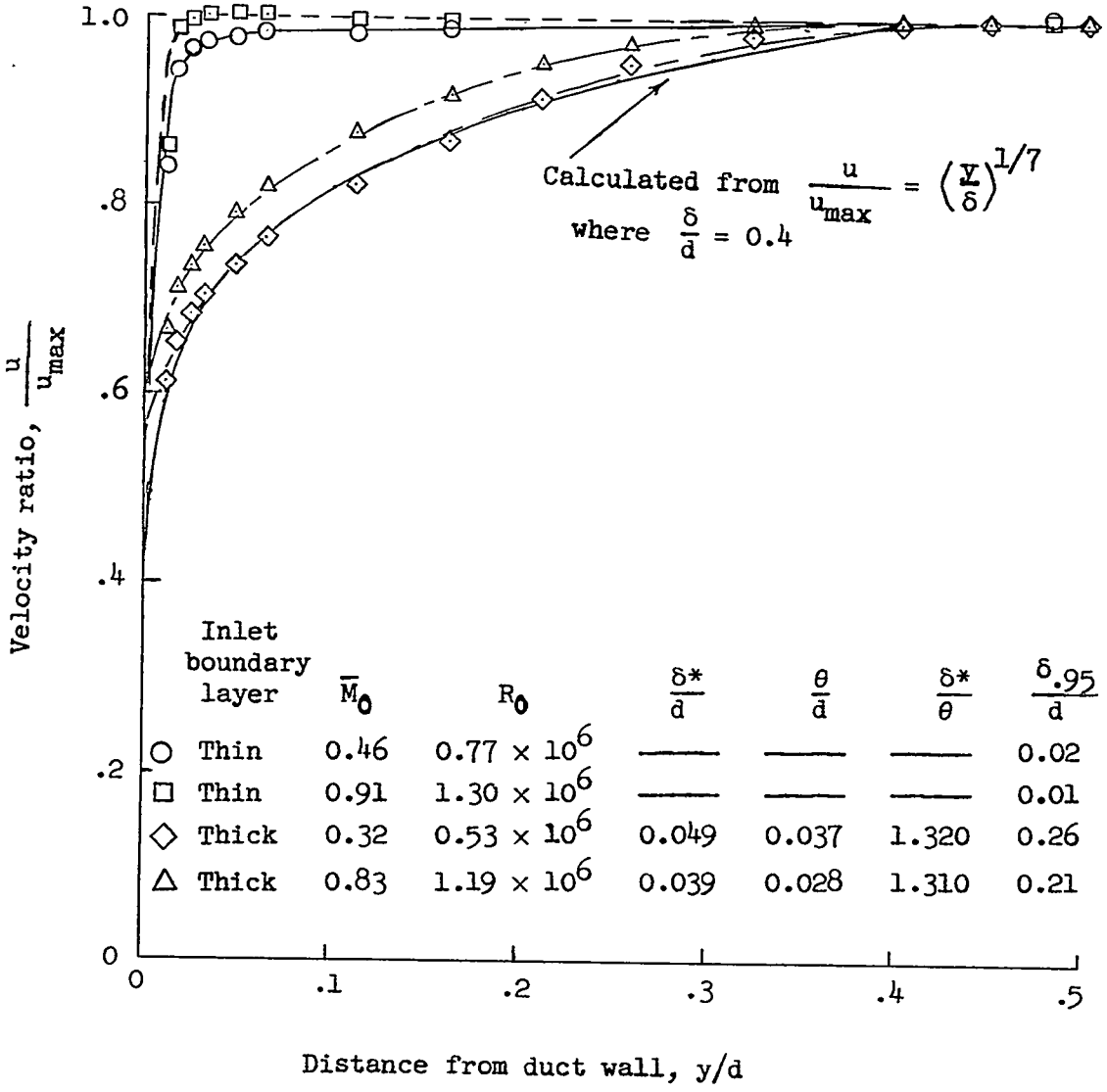

Figure 4.- Velocity profiles at elbow inlet station (station 0) for thin and thick inlet boundary layers.

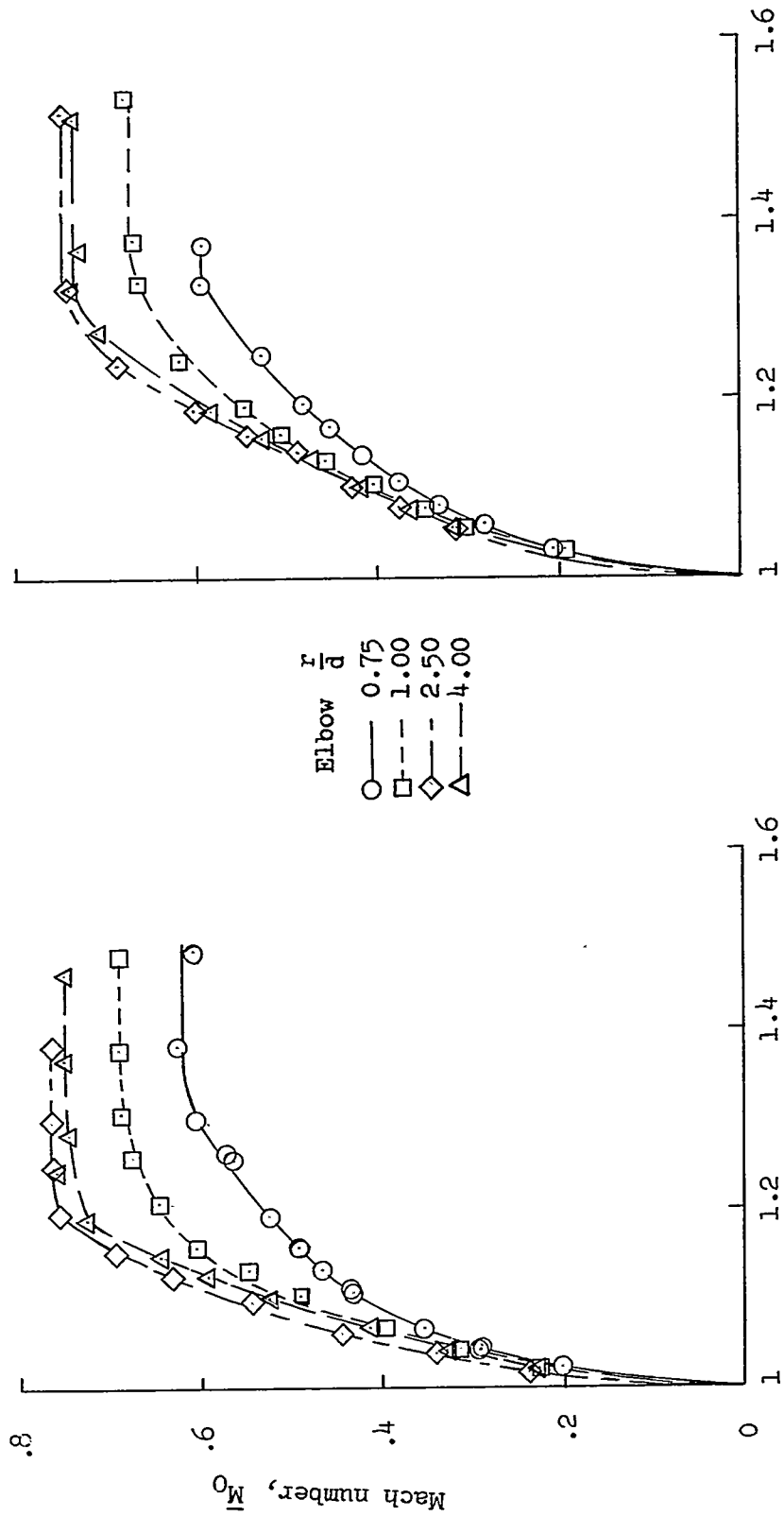

(a) Thin inlet boundary layer. (b) Thick inlet boundary layer.

Figure 5.- Variation of Mach number at station 0 with reference pressure ratio for each elbow for thin and thick inlet boundary layers.

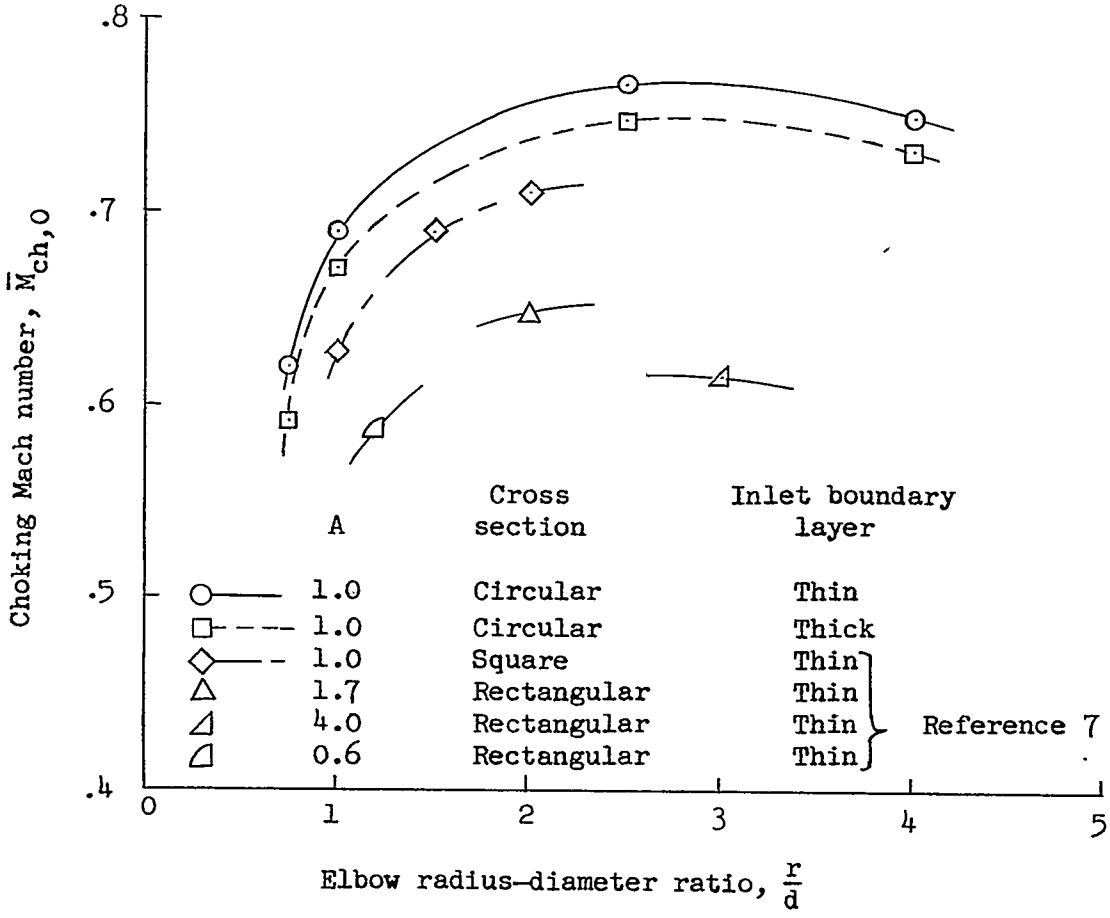

Figure 6.- Variation of choking Mach number at station 0 with ratio of radius of curvature to diameter of the test elbows for thin and thick inlet boundary layers.

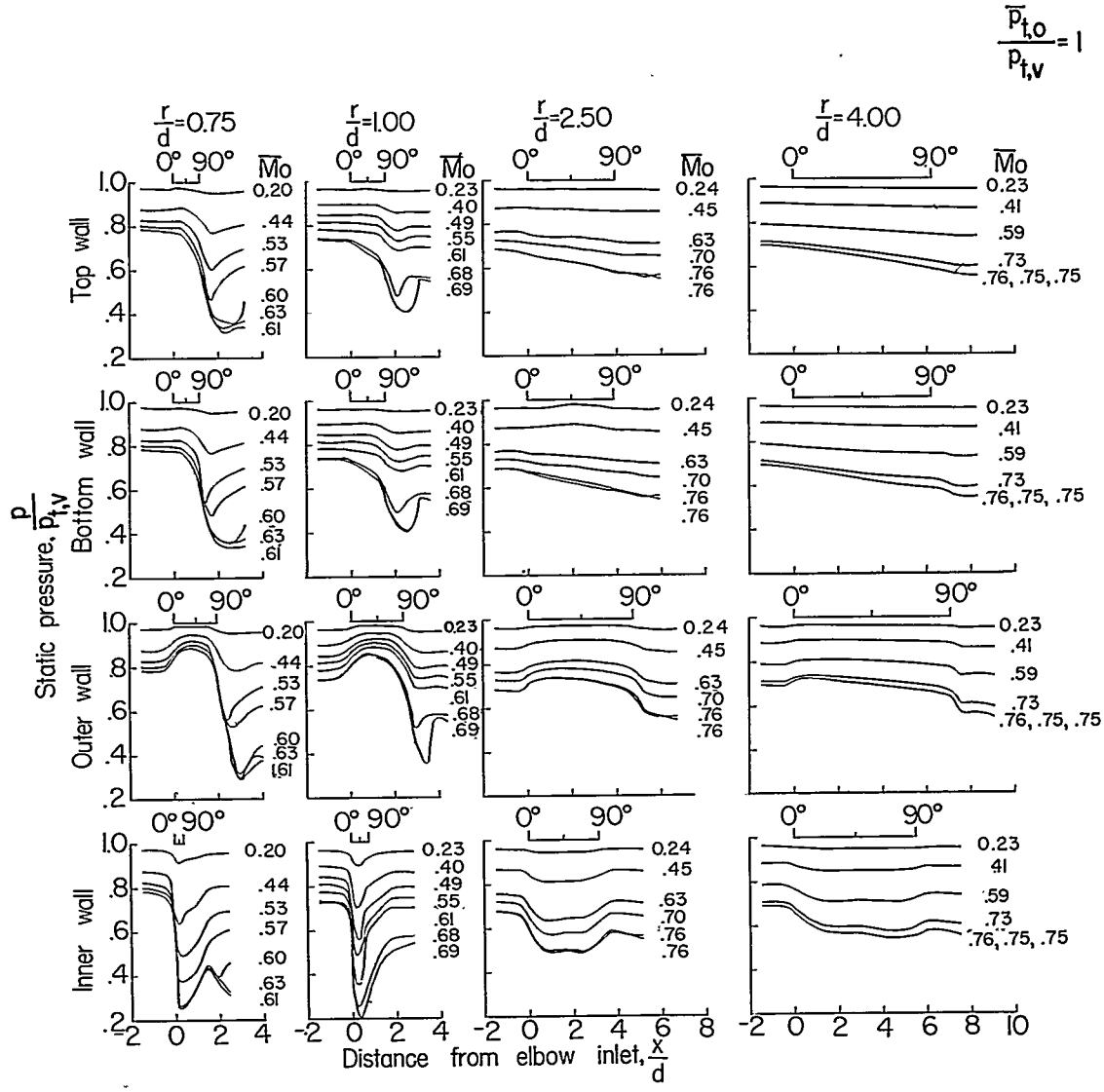

(a) Thin inlet boundary layer.

Figure 7.- Static-pressure distribution through elbows for varying inlet Mach numbers.

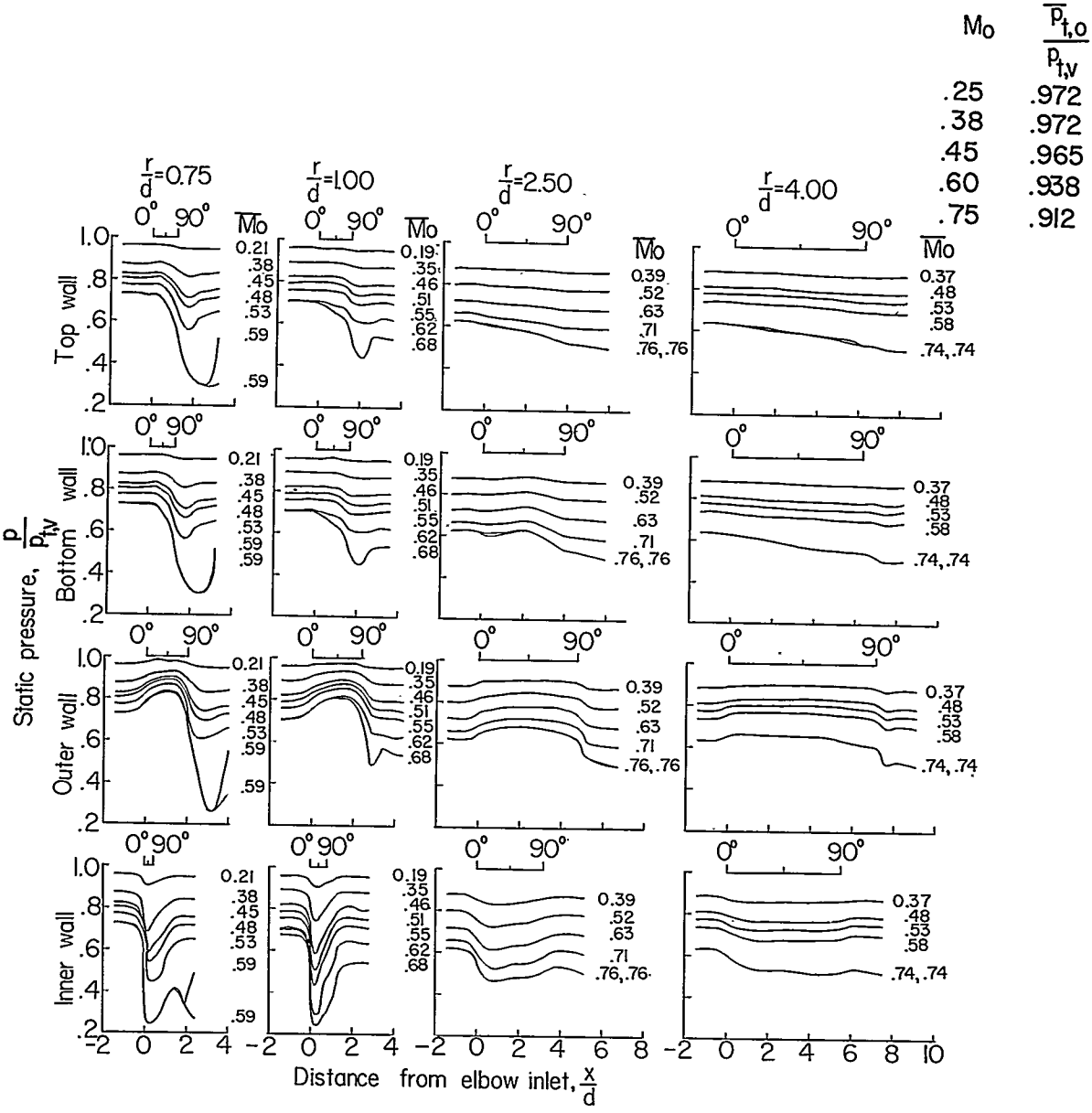

(b) Thick inlet boundary layer.

Figure 7.- Concluded.

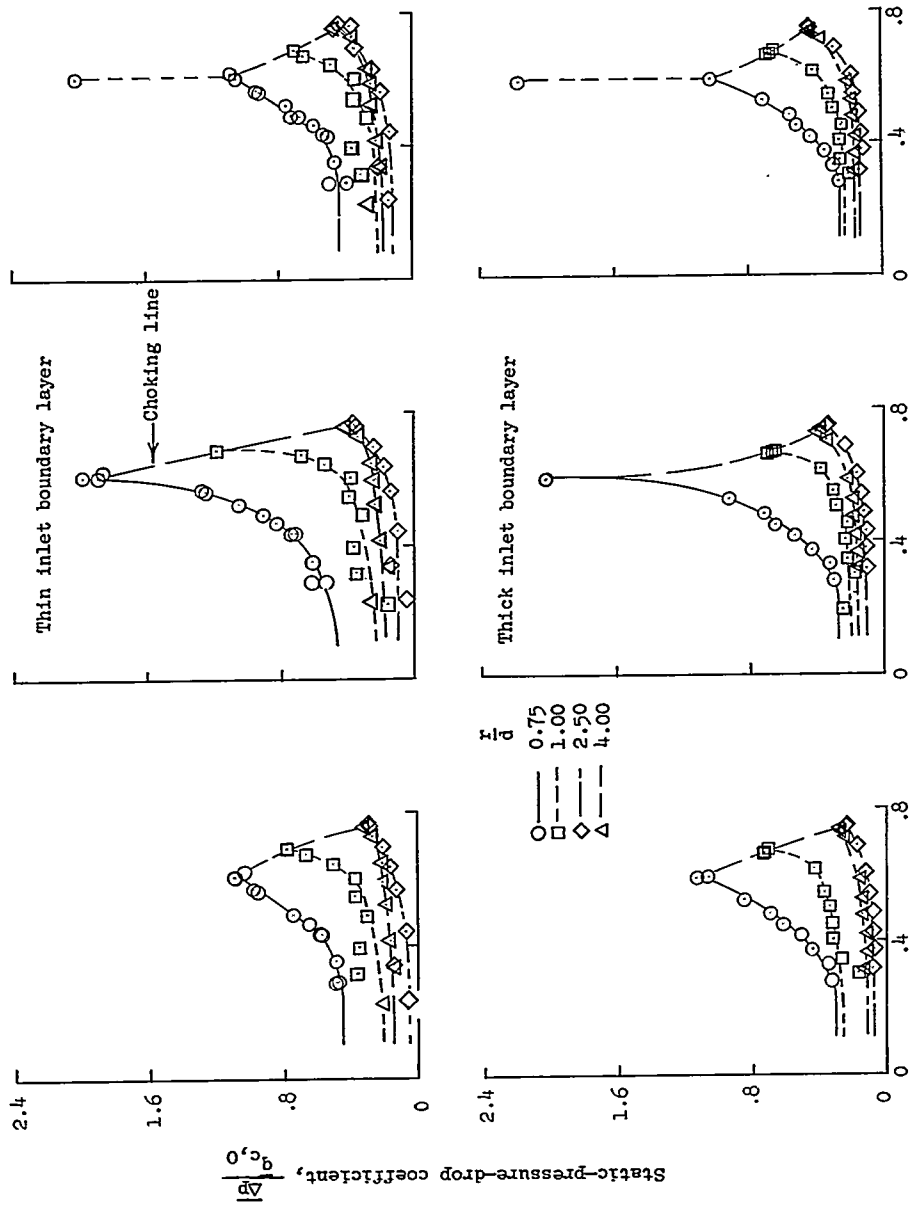

(a) Station e. (b) Station 1.0. (c) Station 2.0.

Figure 8.- Variation of static-pressure-drop coefficient with inlet Mach number for each elbow for thin and thick boundary layers.

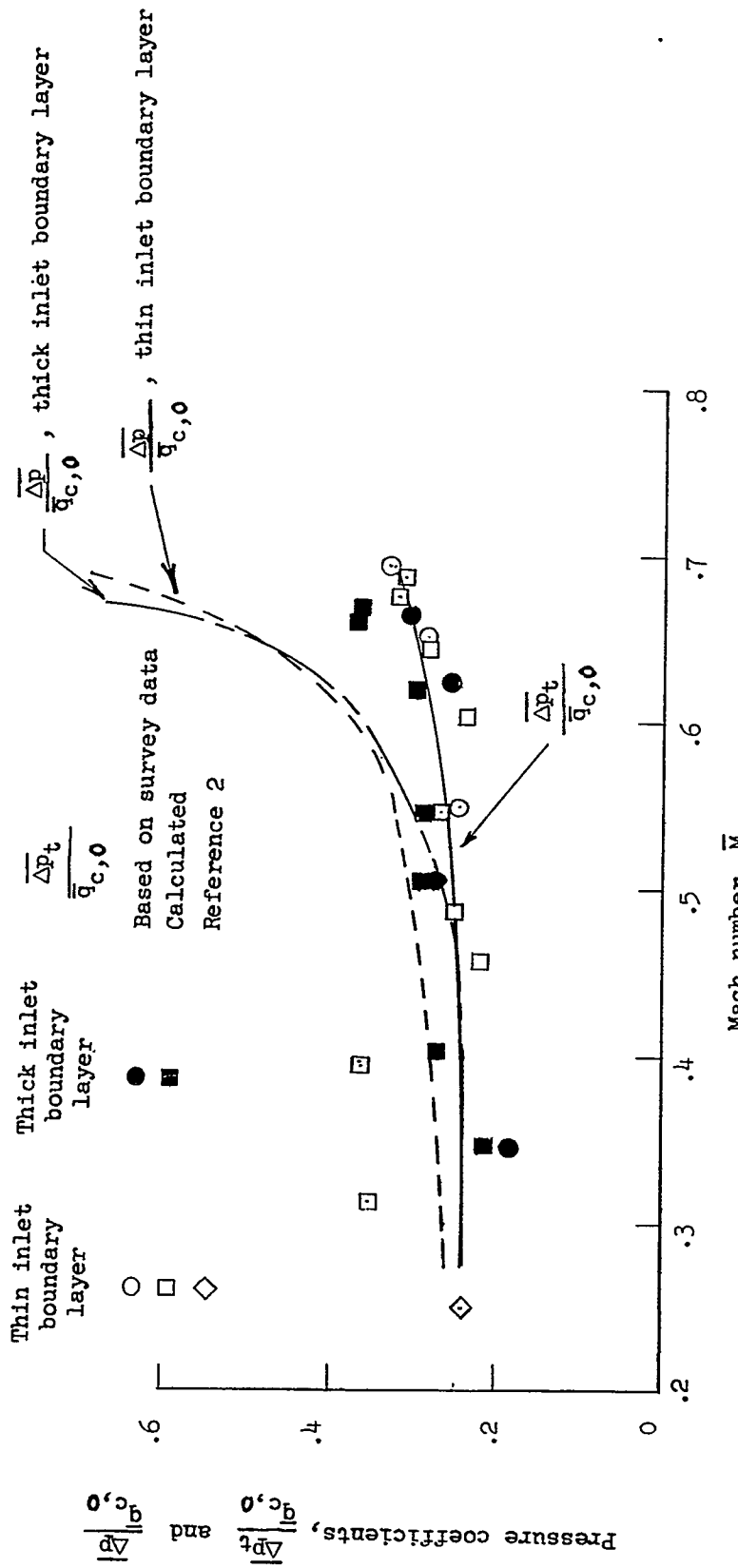

Figure 9.- Variation of the survey and calculated pressure coefficients with Mach number $\bar{M}_0$ from station 0 to station 1.5 for the r/d = 1.00 elbow.

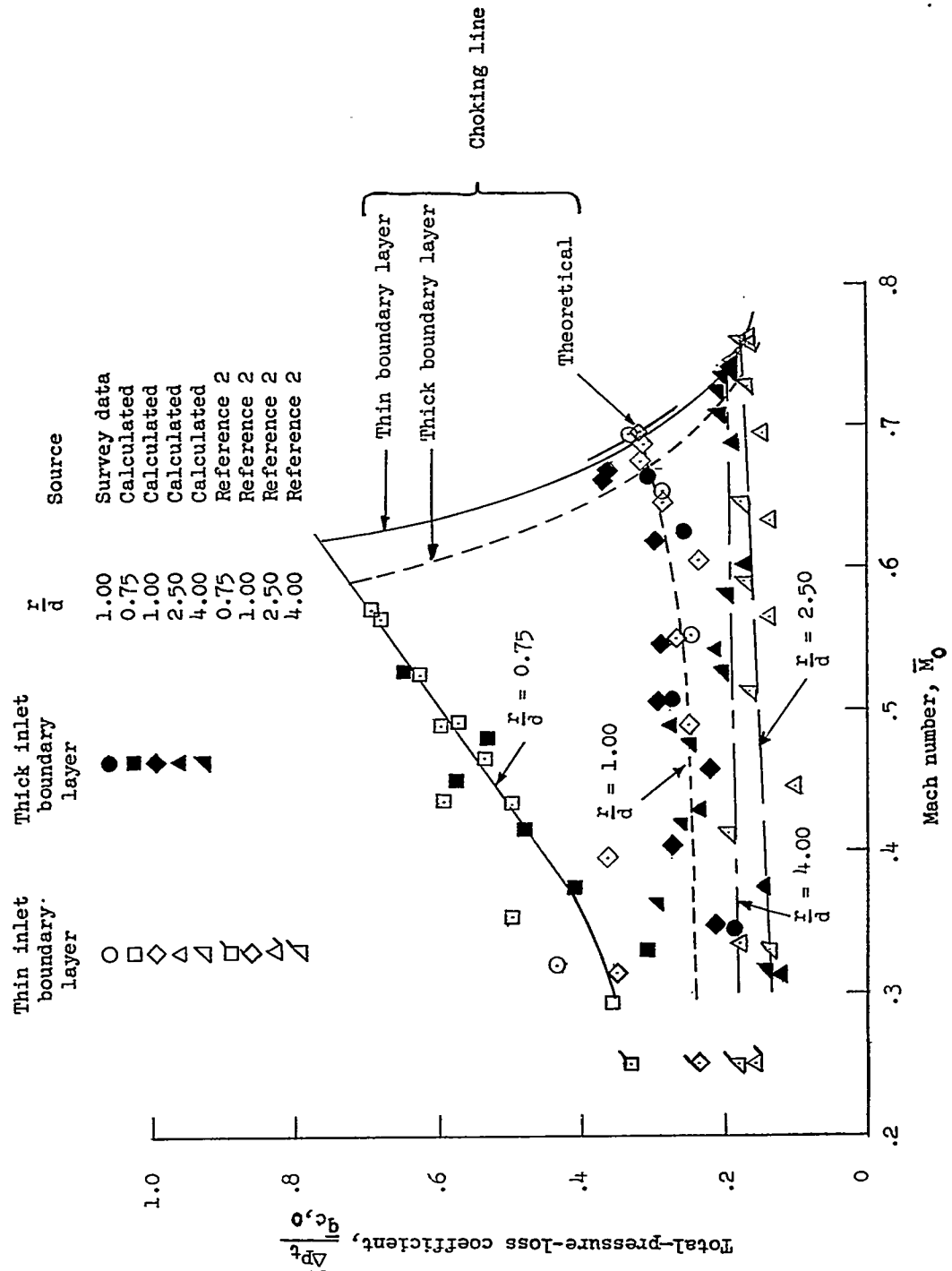

Figure 10.- Variation of total-pressure-loss coefficient at station 1.5 for each elbow.

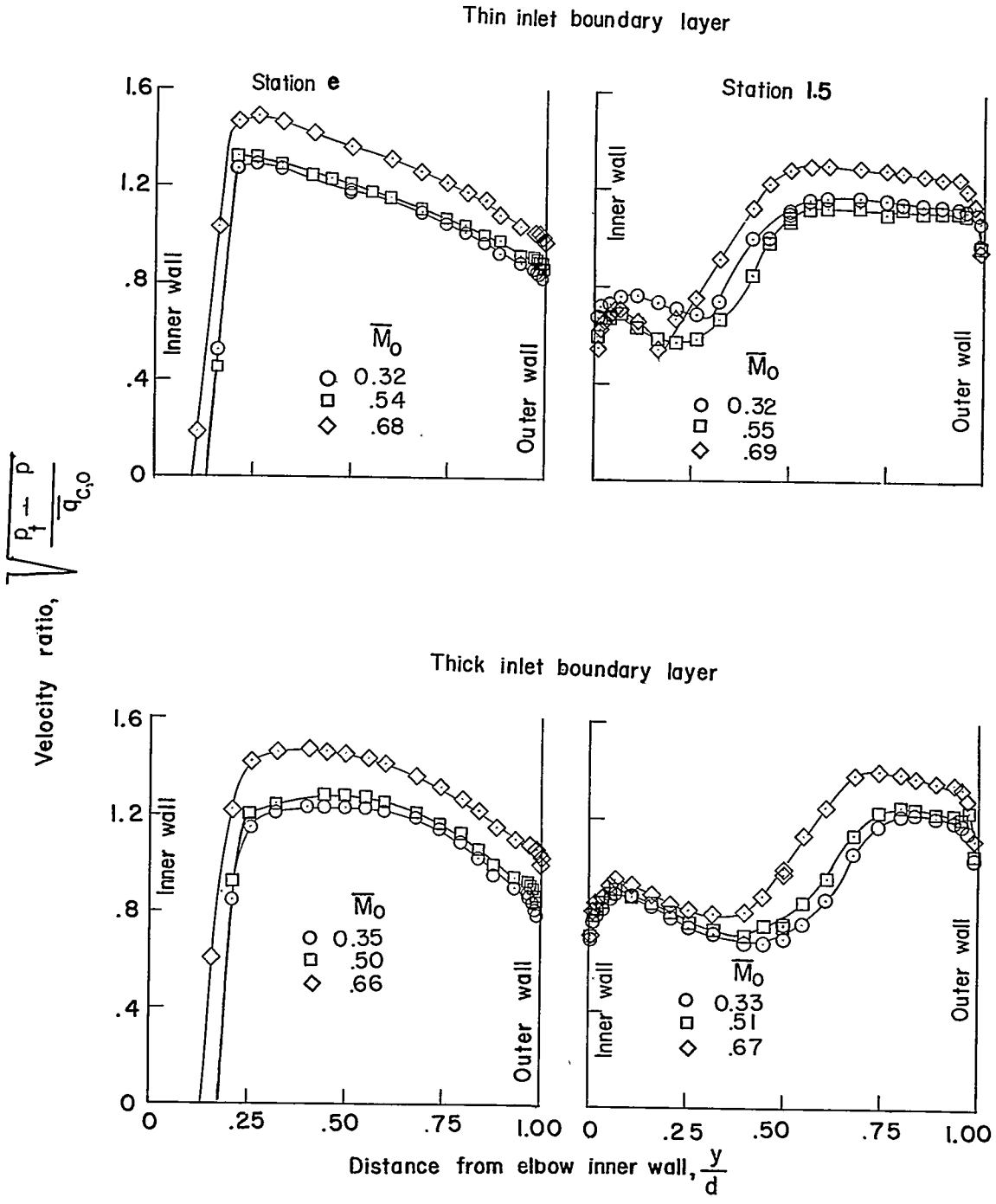

Figure 11.- Variation of local velocity in plane of elbow turning radius, downstream of the r/d = 1.00 elbow at stations e and 1.5.

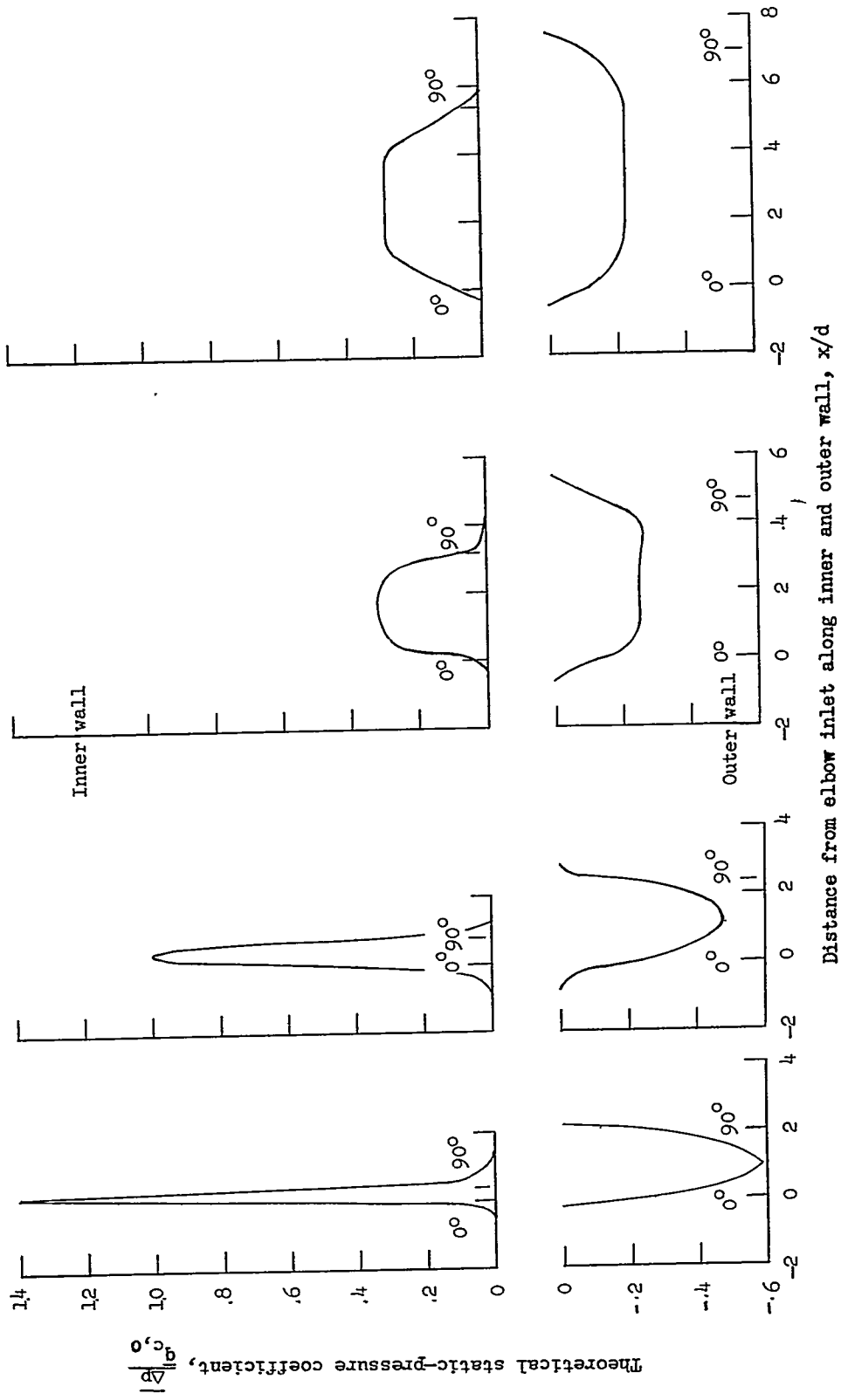

(a) r/d = 0.75. (b) r/d = 1.00. (c) r/d = 2.50. (d) r/d = 4.00.

Figure 12.- Two-dimensional theoretical static-pressure distributions along the inner and outer walls.

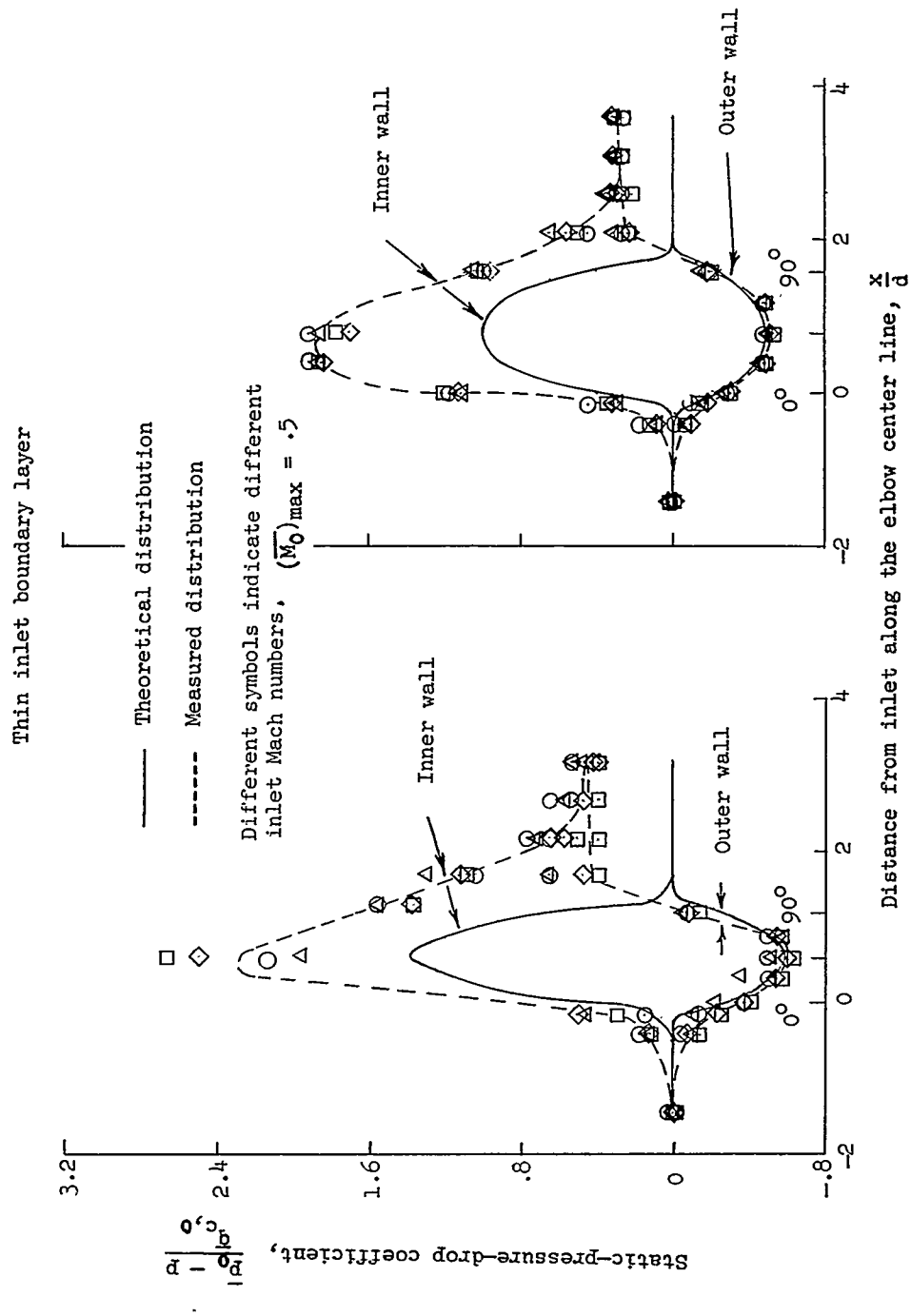

(a) r/d = 0.75. (b) r/d = 1.00.

Figure 13.- Comparison of theoretical static-pressure distributions with distributions measured for thin inlet boundary layer.

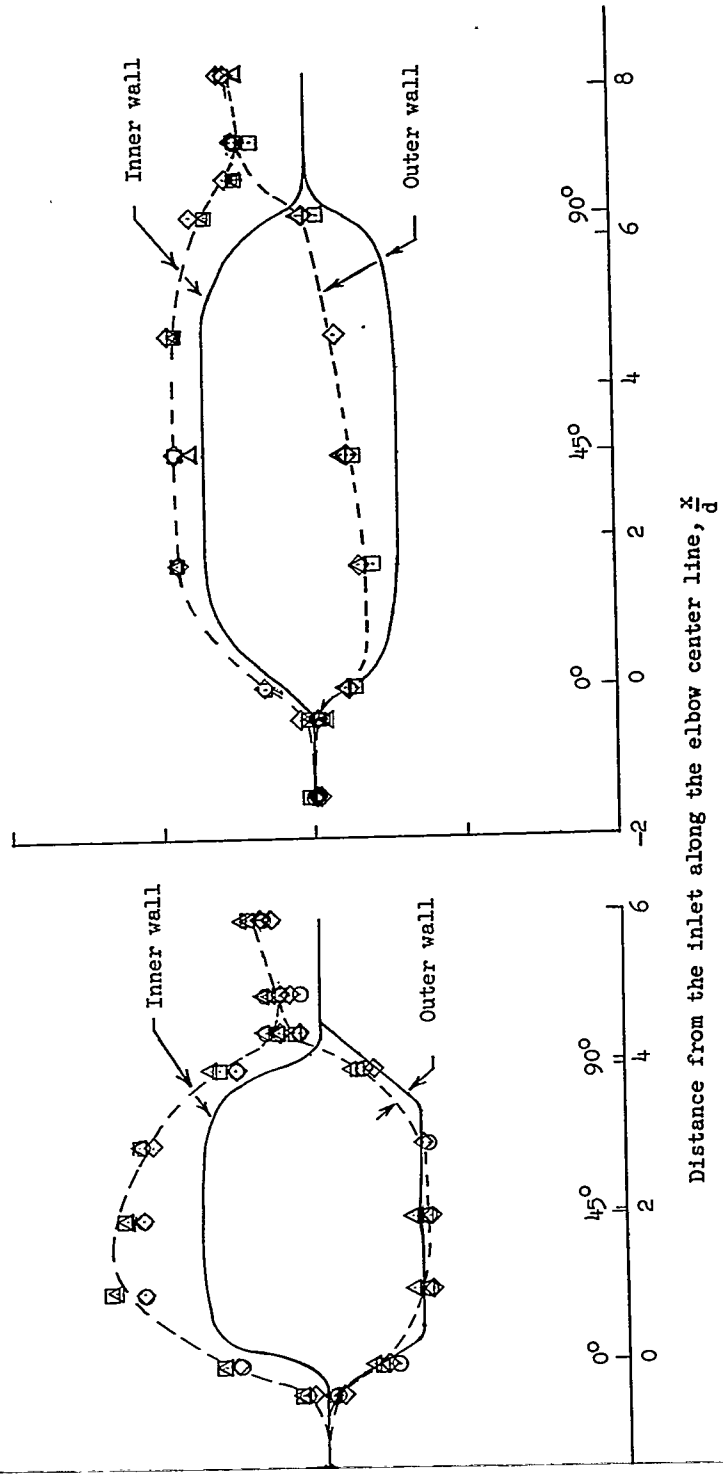

(c) r/d = 2.50.

(d) r/d = 4.00.

Figure 13.- Concluded.